Low efficiency of Janus microswimmers as hydrodynamic mixers

Maximilian R. Bailey [1,*] Dmitry A. Fedosov [2] Federico Paratore [1] Fabio Grillo [1]
Gerhard Gompper [2] and Lucio Isa [1,†]

[1]*Laboratory for Soft Materials and Interfaces, Department of Materials, ETH Zürich, Vladimir-Prelog-Weg 5, 8093 Zürich, Switzerland*
[2]*Theoretical Physics of Living Matter, Institute of Biological Information Processing and Institute for Advanced Simulation, Forschungszentrum Jülich, 52425 Jülich, Germany*

(Received 3 November 2023; revised 21 May 2024; accepted 1 August 2024; published 1 October 2024)

The generation of fluid flows by autophoretic microswimmers has been proposed as a mechanism to enhance mass transport and mixing at the micro- and nanoscale. Here, we experimentally investigate the ability of model 2D active baths of photocatalytic silica-titania Janus microspheres to enhance the diffusivity of tracer particles at different microswimmer densities below the onset of collective behavior. Inspired by the similarities between our experimental findings and previous results for biological microorganisms, we then model our Janus microswimmers using a general squirmer framework, specifically treating them as neutral squirmers. The numerical simulations faithfully capture our observations, offer an insight into the microscopic mechanism underpinning tracer transport, and allow us to expand the parameter space beyond our experimental system. We find strong evidence that near-field interactions dominate enhancements in tracer diffusivity in active Janus baths, leading to the identification of an operating window for enhanced tracer transport by chemical microswimmers based on scaling arguments. Based on this argumentation, we suggest that for many chemically active colloidal systems, hydrodynamics alone is likely to be insufficient to induce appreciable mixing of passive components with large diffusion coefficients.

DOI: 10.1103/PhysRevE.110.044601

I. INTRODUCTION

The ability of active matter to transduce available energy into directed motion has inspired research across various disciplines [1,2]. Among the systems studied at the micron-scale, where Brownian fluctuations and viscous forces are significant [3], the autophoretic motion of chemical microswimmers has been proposed to induce micromixing in fluids [4,5], with potential applications ranging from environmental remediation [6] to synthetic chemistry [7]. Enhancing diffusivity at the microscale has been extensively researched in the context of biological microswimmers [8–15], with possible implications including enhanced nutrient uptake by the microorganisms [16] and even ocean biomixing [17]. At even smaller length scales, active enzyme solutions have been shown to enhance tracer diffusion via momentum transfer [18,19]. Nevertheless, analogous systematic studies of enhanced mixing by synthetic, catalytic microswimmers are lacking [20], except for systems propelled by bubble generation [21,22]. The mixing capabilities of such systems are nevertheless of interest, e.g., for advanced reactor designs incorporating microswimmers, where the use of biological materials or the formation of bubbles may be undesirable, but where mass-transport limitations are important.

Here, we investigate the mixing properties of a widely studied synthetic active matter model system consisting of a suspension of photocatalytically active Janus particles with a titania cap under UV illumination. We overcome the limited scale of conventional Janus particle fabrication techniques via toposelective nanoparticle attachment (TNA), which exploits an emulsion template and multifunctional polymers to facilitate the selective binding of a broad range of nanoparticles, including the photocatalytic titania nanoparticles used in this study, onto silica particle supports [23,24]. The advantages of TNA not only lie in the greater than 100 mg yields per batch, which ensures reproducibility between experiments [25], but also the scalability and modularity offered in catalyst selection, which is desirable from an applications perspective. While experimentally probing the mechanisms leading to the enhanced transport of passive tracers, we observe parallels between their dynamics in active baths of our synthetic active colloids and previous findings for biological microswimmers [9,14,26]—despite their vastly different underlying propulsion schemes. Specifically, the passive particles demonstrate Lévy flight-like trajectories [16], characterized by diffusive displacements interdispersed with large translational jumps.

Drawing on the concept of active flux [20,27,28], we determine a positive correlation between the timescale expected for swimmers to interact with the passive tracers via hard-core and near-field hydrodynamic interactions [10,12,26,29,30], and the peak in the non-Gaussian parameter attributable to the tails in the distribution of displacements arising from tracer jumps [14]. We then use a coarse-grained hydrodynamic swimmer model—a squirmer which is equivalent to a force dipole and source dipole in the far field—to capture the generic aspects of tracer mixing [31,32]. Noting the good qualitative agreement between numerical simulations and experiments, we proceed to study the mixing properties of our

*Contact author: maximilian.bailey@empa.ch
†Contact author: lucio.isa@mat.ethz.ch

hydrodynamic squirmers under conditions beyond those experimentally achievable, and observe a linear scaling in the diffusivity enhancement of our tracers with the active flux of the squirmers [8,9,27]. Making use of dimensionless quantities, we conclude by highlighting several key considerations for the design of catalytic microstirrers.

II. RESULTS

A. Experimental system

Our microswimmers are spherical SiO_2 colloids (diameter $d_{\text{swim}} = 2.16\mu\text{m}$) half decorated with photocatalytic TiO_2 nanoparticles, as described in detail in Refs. [23,24]. Under UV illumination, the particles asymmetrically degrade H_2O_2 (fuel) and thus establish local chemical gradients, leading to self-propulsion by autophoresis [33–37]. The density mismatch of the particles, coupled with the experimental conditions used (see Supplemental Material, Materials and Methods [38]) minimizes their out-of-plane motion away from the substrate [39,40] and ensures that particles move in two dimensions (2D xy plane). Under these conditions, we systematically study the behavior of the microswimmers as their effective area fraction $\Phi_{\text{swim}} = N_{\text{swim}}A_p/A_T$, where N_{swim} is the number of microswimmers, $A_p = \pi d_{\text{swim}}^2/4$ is the 2D projection of the microswimmer area, and A_T is the area of the system, is varied. In agreement with previous reports for both synthetic and biological systems [41–49], we observe the formation of dynamic clusters" above a threshold swimmer density (see Supplemental Material, Fig. S1, and Videos S1 and S2 [38]). The emergence of collective behavior, although of significant fundamental interest, not only complicates the analysis of the mixing properties of microswimmers but also likely hinders their overall mixing efficiency [50], as we outline below. We therefore determine the limiting area fraction of microswimmers before the onset of clustering events using the methodology outlined by Theurkauff *et al.* [41] (see Supplemental Material, Fig. S1a [38]). In agreement with their findings, we determine an onset of clustering at $\Phi_{\text{swim}} \approx 0.05$ (see Supplemental Material, Fig. S1c [38]), which we thus set as the upper bound for our experiments to focus on single-particle effects. Similar to the seminal work by Wu and Libchaber [8] on the mixing properties of bacterial baths, the speed distribution of our synthetic free" particles obeys Maxwell's statistics, however, in its 2D form as particle motion is confined above the substrate: $P(V_0) = \frac{V_0}{v_M^2}\exp(-\frac{V_0^2}{2v_M^2})$, where v_M is the modal speed. Under the experimental conditions used, our active colloids have a modal speed $v_M \approx 3.1\mu\text{ms}^{-1}$ [see Fig. 1(b)].

B. Tracer dynamics

Having established the upper bound for the number density of our microswimmer baths, we investigate the effect of microswimmers on the dynamics of micron-sized tracers (diameter $d_T = 1.70\,\mu\text{m}$). Notably, we find that the tracers display extensive displacements when a microswimmer passes in their vicinity [Fig. 2(a), Supplemental Material Video S3 [38]), which we henceforth refer to as jumps. We underline that these enhancements in the motion of the tracers are distinct to previous studies on colloidal transport, where the microswimmer actively transports the tracer by making use of phoretic or hydrodynamic effects to drag the tracer along its trajectory [51–53] (also see Supplemental Material Fig. S2 on the overweighted effect such transported tracers can have on the ensemble mean-squared displacement (EMSD) [38]). In contrast, the jumps do not require that the tracer is effectively carried by the microswimmer, and instead extended displacements are also observed in directions distinct from the velocity of the microswimmers (see Supplemental Material, Video S3 [38]).The presence of these large displacements, which result in trajectories reminiscent of Levy flights [16], is well established for passive tracers in the presence of different suspensions of micro-organisms [8,9,14,28], and is attributed to the velocity flow fields created by their motion [12,13,17]. We, however, note the absence of previously observed loops in our observed tracer trajectories, potentially arising from the flow-distorting effect of the wall above which the particles move [27] or from the effect of near-field hydrodynamic and steric interactions [10,14,15,29,54].

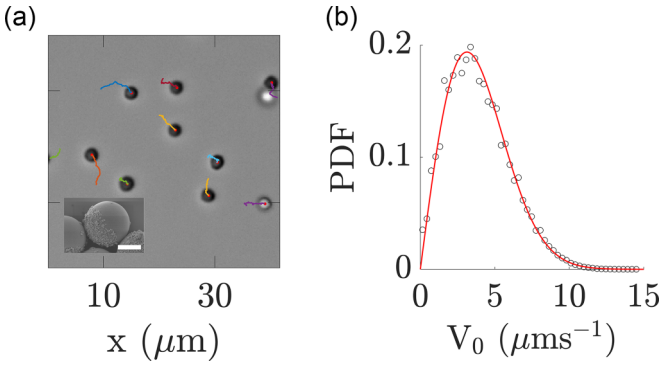

FIG. 1. Janus microswimmer 2D motion above a substrate in the absence of clustering. (a) Micrograph of free particles at low area fraction $\Phi_{\text{swim}} = 0.02$ (1 s trajectory). Inset: HR-SEM image of the studied Janus particles. Scale bar represents 1 μm. (b) Distribution of the free microswimmer in-plane speeds measured over 40 000 trajectories.

C. Hydrodynamic mixing via active flux

Via simple scaling arguments, we now seek to demonstrate that these tracer jumps are at least in part caused by near-field hydrodynamic and hard-core interactions between the tracers and the microswimmers. We begin with the concept of the active flux of microswimmers, proposed by Miño *et al.* [20,27] as $J_{\text{swim}} = \phi_{\text{swim}} \cdot \langle V_0 \rangle$, where $\phi_{\text{swim}} = N_{\text{swim}}/A_T$ is the number density of microswimmers and $\langle V_0 \rangle$ is their mean speed. Assuming that the N_{trac} passive tracers in the system are equidistantly distributed, it follows that the characteristic length scale between tracers can be written as $1/\sqrt{\phi_{\text{trac}}}$, where $\phi_{\text{trac}} = N_{\text{trac}}/A_T$ is the number density of tracer particles. Given these definitions, we then identify a characteristic time $\tau_c = \sqrt{\phi_{\text{trac}}}/J_{\text{swim}}$ for near-field interactions between a microswimmer-tracer pair, i.e., the time expected for a swimmer to travel the intertracer distance, given the activity flux. Returning to the tracer jumps, these larger displacements are expected to dominate the higher

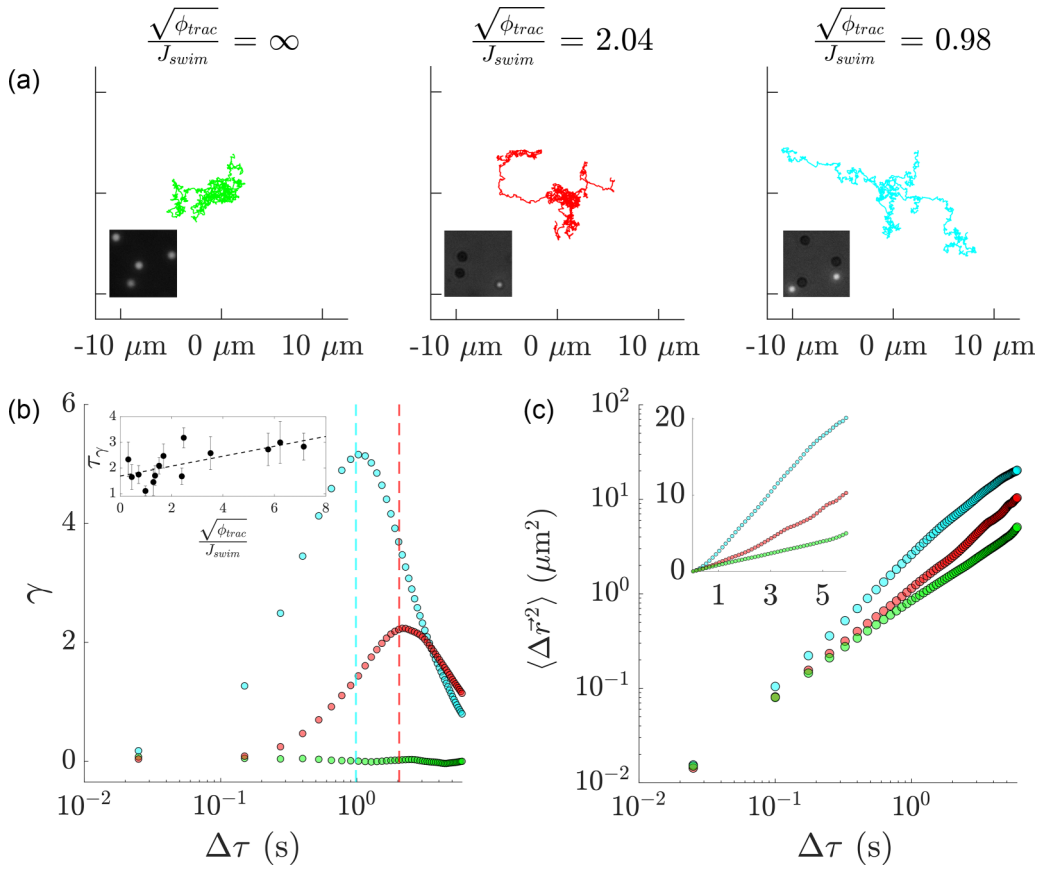

FIG. 2. Emergence of large displacements in the trajectories of tracers with the introduction of microswimmers. (a) Tracer trajectories for three different experimental cases corresponding to various $\sqrt{\phi_{\text{trac}}}/J_{\text{swim}}$ [green (left): infinity; red (middle): 2.04 s; cyan (right): 0.98 s]. Scale bars represent 5 μm. Insets are representative snapshots of the experimental system (bright tracers and dark microswimmers, 16.25 x 16.25 μm). (b). Evolution of the kurtosis γ of the distribution of displacements with lag time $\Delta\tau$ for the three experimental conditions depicted in (a). [From bottom to top, the Kurtosis curves correspond to green (bottom); red (middle); and cyan, (top trajectories)]. Each data set contains at least 23 trajectories. The dashed lines indicate $\sqrt{\phi_{\text{trac}}}/J_{\text{swim}}$ for the given experimental conditions. Inset: Correlation between the estimated near-field interaction time $\sqrt{\phi_{\text{trac}}}/J_{\text{swim}}$ between a tracer and a swimmer and the experimentally observed lag time at which the kurtosis is maximised. Error bars indicate the standard error of the mean. (c) Ensemble mean-squared-displacement (EMSD) of the three experimental systems depicted in (a). (From bottom to top, the EMSD curves correspond to green, bottom; red, middle; cyan, top trajectories.)

orders of the distribution of tracer displacements, i.e., its kurtosis ($\gamma = \langle(\Delta x - \langle\Delta x\rangle)^4\rangle / \langle(\Delta x - \langle\Delta x\rangle)^2\rangle^2 - 3$), due to their higher weighting for larger powers [14,26]. Here, Δx denotes the one-dimensional (1D) independent displacements of the tracers in x and y, which are then binned together for increased statistics. Extracting γ from the tracers for different experimental realizations of τ_c, we find a positive correlation between τ_c and τ_γ, the lag-time τ at which γ is at a maximum [see Fig. 2(b)]. We obtain this value by fitting a smoothing spline to $\gamma(\tau)$ and obtaining the τ value at which γ is maximized. As τ_c decreases, and swimmer-tracer collisions become more prevalent, the overall diffusivity of the tracers is also enhanced, as can be detected in their EMSD [see Fig. 2(c)].

Further evidence for the enhancement in tracer diffusivity as a result of tracer jumps is presented in Fig. 3 (top row). Following Jeanneret *et al.* [14], we distinguish between standard diffusive motion during a fixed time and jumps, using the autocorrelation of subsequent displacements. Although the significantly lower speeds of the studied synthetic microswimmers reduces the effective size of the tracer jumps, it is clear that long-time exponential tails emerge in the distribution of tracer displacements when jumps are included, replicating the findings for microalgae [14]. Rescaling the distribution of displacements at intermediate lag times by the square root of the lag-time $\sqrt{\tau}$ causes their collapse onto a single curve. This diffusive scaling, observed in active baths of eukaryotic microorganisms [9], is attributed to the effect of near-field interactions which cause large displacements, i.e., jumps, which dominate higher order moments of the distribution at intermediate times [26]. We therefore hypothesize that near-field interactions between Janus microswimmers and passive particles, resulting in large tracer displacements, play a dominant role in enhancing their diffusivity. Far-field flows, if generated by the microswimmers, may, in fact, be dampened by the presence of the underlying substrate, which can dissipate the generated flows [13,27].

The qualitative agreement between our findings and those for microorganisms was not expected *a priori*, but provides us with the opportunity to use theory developed for such systems to describe our own. Specifically, the squirmer model [31], initially proposed for microorganisms [55,56], is frequently

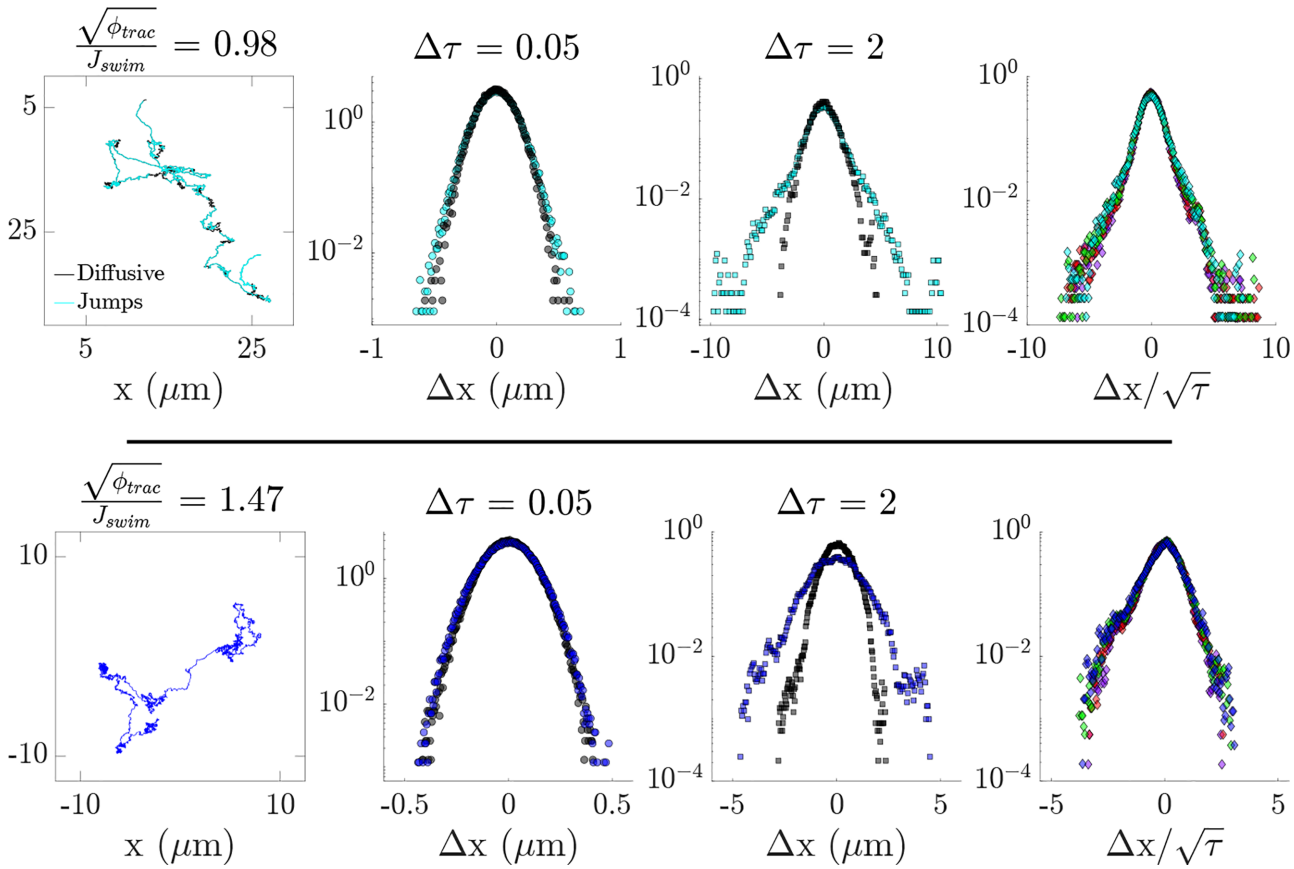

FIG. 3. Influence of the jumps on the tracer distribution of displacements at different lag times $\Delta\tau$. (●) and (■) refer to experiments; (●) and (■) refer to simulations; (●) and (■) correspond to the diffusive parts of the trajectories for both experiments and simulations. Top row: Experimental tracer trajectory in a microswimmer bath. The non-Gaussian, exponential tails in the distribution of displacements becomes prominent at longer lag times. We note that these tails are not observed for passive microswimmers (see Supplemental Material, Fig. S3 [38]). Bottom row: Our numerical neutral squirmer model maps qualitatively well onto the experimental findings, with the presence of jumps at longer $\Delta\tau$ seen in the tails of the distribution of displacements. In both experiments and simulations, we observe diffusive scaling with $\sqrt{\tau}$ [9], which is attributed to the intermediate values of τ studied where the near field dominates [26]. (♦) $\tau = 0.75$s, (♦) $\tau = 1$s, (♦) $\tau = 1.5$s, (♦) $\tau = 2$s: experiments. (♦) $\tau = 2$s: simulations. All symbols are plotted with 80% transparency for better visualization.

invoked to describe the flow fields surrounding chemical Janus microswimmers [32,40,57] and generates flows which are consistent with a coarse-grained framework incorporating hydrodynamic effects in the far field via a multipole expansion, together with appropriate near-field fluid flows. We note that a more complete description of chemically active colloids requires the analysis of the phoretic flows resulting from the chemical gradients produced by the microswimmers [58,59] (see Supplemental Material, Fig. S4 [38]). Still, a complete description of the phoretic and osmotic flows requires the relevant mobility parameters—reducing generalizability to other mixing systems. For a coarse-grained model to describe the mixing properties of our microswimmers, we therefore neglect the phoretic contribution to tracer displacements, following Ref. [60] (also see Supplemental Material, Fig. S5 [38]).

D. Numerical simulations

We begin by modeling our synthetic microswimmers as neutral squirmers (squirmer parameter $\beta = 0$—see Supplemental Material, Materials and Methods for a detailed description of the simulation method and description of parameters [38]), informed by previous work on catalytic Janus particles [61], and the dominant role of near-field interactions predicted for such systems in enhancing tracer diffusivity [12,29]. The neutral squirmer model furthermore agrees with the absence of transport behaviors associated with flow vortices [62] and the absence of long-range forces observed [29] (see Supplemental Material, Fig. S5 [38]). Fluid flow is modeled using dissipative particle dynamics (DPD), a mesoscopic hydrodynamics simulation technique where the fluid is represented by a large but finite number of solvent particles. In DPD, stochastic and dissipative forces are introduced to act as a thermostat [63,64]. Here, both passive and active colloids consist of particles placed homogeneously on a spherical surface, connected by bands to form a triangulated mesh, to ensure a near-rigid shape (see Supplemental Material, Materials and Methods for more details [38]). Propulsion is modeled by imposing a slip velocity at the surface of the active particles using the spherical squirmer model [65] and solving Newton's equations of motion using the velocity-Verlet algorithm. For

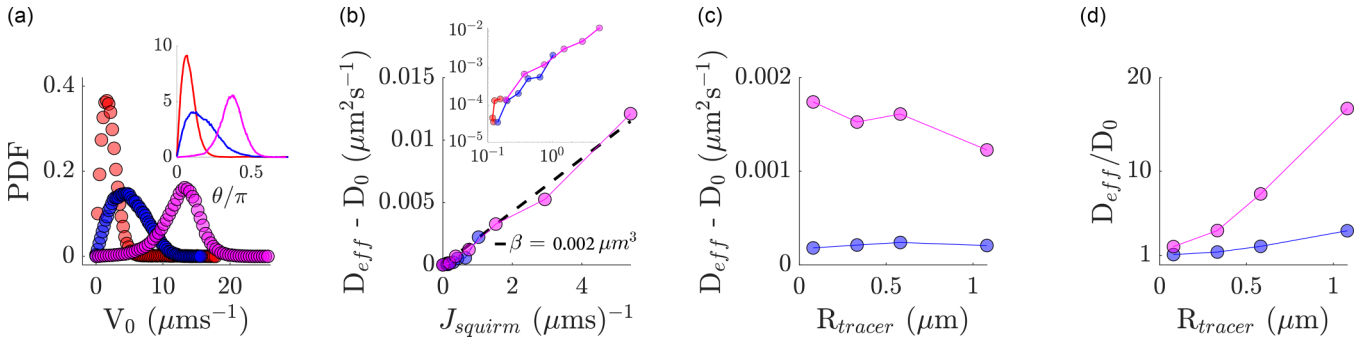

FIG. 4. Dynamics of simulated active and tracer particles [red (left) for pullers, blue (middle) for neutrals, and magenta (right) for pushers.] (a) Distributions of squirmer in-plane (2D) speeds for fixed squirmer strengths (all types would have the same swimming speed under unbounded conditions). Inset: Orientation distributions of active and tracer particles with respect to the z axis (i.e., perpendicular to the wall). (b) Increase in the diffusion coefficient of the tracers, D_{eff}–D_0, with increasing squirmer flux J_{squirm}. The dashed line indicates a linear least-squares fit for the pushers. Inset: Log-log plot for visualization of data points. Data set for pullers is limited, as with increasing swimming strength they become immobilized on the substrate. (c) The enhancement in the tracer diffusion coefficient for pushers (top) and neutral squirmers (bottom), D_{eff}–D_0 is relatively flat across different tracer sizes [9,13,20,27], for pushers, the slight increase with decreasing size may arise from the growing role of tracer entrainment [13,29]. (d) Normalized enhancement in the diffusion coefficient, D_{eff}/D_0, for different sizes of passive tracers for pushers (top) and neutral squirmers (bottom).

passive particles, no-slip boundary conditions (BCs) are imposed. To relate simulation and physical units, we introduce characteristic length and time scales. The length scale is based on the squirmer diameter $d_{Sq} = 2.16\,\mu$m, as in experiments, and the timescale is set by $\tau_{Sq} = d_{Sq}/v_M$, where v_M is the modal value of the speed distribution of active particles in the xy plane previously calculated [see Fig. 1(b)], which is set as the squirmer speed. In this manner, the simulation domain is set to 33.2 x 33.2 x 6.8 μm with periodic BCs in the xy plane, and walls at z = 0 and z = 6.8 μm. Rigid walls are simulated by immobilised DPD particles having identical number density and interactions as the fluid particles. The immobile wall particles enforce no-slip BCs at the walls through dissipative interactions with the fluid particles. To prevent wall penetration by fluid particles, reflective surfaces are introduced at the interface between the fluid and the walls. Both passive and active particles are confined within a layer of 2.45 μm at the lower wall with no-slip BCs to mimic the quasi 2D setup in the experiments. The wall at z = 6.8 μm assumes slip BCs to better capture experimental conditions. The area fraction of active particles corresponds to $\Phi_{swim} = 0.0597$, identified as the approximate onset of clustering in both experiments and simulations.

We find that the dynamics of our simulated passive tracer particles in the presence of neutral squirmers are qualitatively very similar to our experimental findings under the same conditions. Specifically, we identify the presence of jumps in the tracer trajectories, which emerge at longer lag times in the distribution of tracer displacements, as well as their diffusive scaling at the same intermediate lag times investigated experimentally (see Fig. 3, bottom row). We note that the magnitude of the displacements determined in numerical simulations are approximately half that observed in experiments, which may be attributed to the role of phoretic flows or finer details of the near-field hydrodynamics of our synthetic microswimmers not incorporated in our coarse-grained model. Nevertheless, encouraged by the good agreement between experiment and simulation, we proceed to a more quantitative characterization of the mixing efficiencies of different squirmers, not only for neutral squirmers ($\beta = 0$) but now also for pullers ($\beta = 5$) and pushers ($\beta = -5$). Here, $\beta = B_2/B_1$, where B_n are cofefficients of the two surface velocity modes. B_1 is the strength of source dipole, which determines the squirmer propulsion velocity ($v = 2B_1/3$ for the case of unconfined spherical squirmers). B_2 is the strength of the force dipole, which introduces a fore-aft asymmetry in the slip velocity field of the squirmer (see Supplemental Material, Materials and Methods for more details [38]). As a control, we also study the dynamics of tracer particles in the presence of particles that do not swim (i.e., passive particles). For a given propulsion strength B_1 selected to mirror experimental speeds, we find that pushers are superior mixers to other squirmer types under the same numerical conditions. However, we note that for a given propulsion strength, the three squirmer types can have significantly different swimming speeds [see Fig. 4(a)]. Upon closer inspection, we find that the discrepancy in swimming speeds is a result of their orientation with respect to the substrate]see Fi. 4(a), inset]. It is well-known that pushers will align parallel to a substrate (resulting in higher speeds), whereas pullers will orient perpendicular to surfaces [66]. Neutral squirmers, in contrast, possess characteristics of both squirmer types, reflected in their intermediate orientation with the substrate, resulting in a distribution of swimming speeds mirroring that observed for our experimental synthetic microswimmers [compare Figs. 1(b) and 4(a)]. By instead comparing the long-term enhanced diffusion coefficient D_{eff}–D_0 (where D_{eff} is the coefficient in the presence of the swimming squirmers, and D_0 is the diffusion coefficient measured in the absence of squirmer activity) with the active flux of the squirmer J_{squirm}, we observe a collapse onto the expected linear scaling given by D_{eff}–$D_0 = \alpha J_{squirm}$ [16,20,27,28], with $\alpha \approx 2 \times 10^{-3}\,\mathrm{m}^3$ or $(0.126\,\mathrm{m})^3$ [see Fig. 4(b)]. We note that this value for α is approximately one order of magnitude less than that previously calculated for active rods and bacteria [20,27].

We then study the effect of reducing the tracer size, R_{tracer}, for squirmers with swimming speeds approximately equal to that determined for our Janus microswimmer system. In agreement with previous investigations [13,20,27,28], we find that tracer size has a relatively small effect on the increase in its long-term diffusion coefficient for a given activity flux [see Fig. 4(c)]. The small enhancement observed for decreasing tracer sizes in the case of pushers could be attributed to the mechanism of entrainment, as the smaller tracers are able to closer approach the squirmer body [13,29]. However, upon rescaling the enhanced tracer diffusivity D_{eff} by the underlying diffusivity of the tracers D_0, we see a clear reduction in the ability of the squirmers to mix small tracers [see Fig. 4(d)]. We thus hypothesize that the mixing capacity of microswimmers is limited by the relative size and frequency of the imparted jumps via near-field interactions compared to the underlying diffusivity of the component to be mixed (i.e., $l_j \gg \sqrt{\mathrm{D}_0 \tau_c}$ for enhanced mixing, where l_j is the jump length after an interaction occurring with frequency $1/\tau_c$). This mirrors the experimental findings using 230 nm nanoparticle tracers where no enhancement in D_{eff} over D_0 was observed (see Supplemental Material Figs. S6 and S7 [38]), suggesting the unsuitability of this type of microswimmer systems to mix, e.g., species with very high diffusion coefficients.

E. Mass-transport considerations

Additional challenges facing the application of micron-scale synthetic microswimmers to overcome mass-transport limitations can be identified by following Purcell's example and evaluating the relevant dimensionless numbers [67–69]. Presuming low Reynolds number conditions, i.e., $\mathrm{Re} = vl/\nu \ll 1$, where ν is the kinematic viscosity and vl relates to the fluid flow at a characteristic length scale l for microswimmers swimming with speed v (i.e., motion in the viscous regime and ignoring substrate effects), we begin with the strength of swimming to thermal diffusion, $\mathrm{Pe} = vl/D$, where D is the translational diffusion coefficient of the transported species. Ignoring hydrodynamic interactions (i.e., only accounting for activity and excluded volume effects), Burkholder and Brady [30] demonstrated that for large values of Pe, steric collisions between the active Brownian particles and passive probe lead to enhanced diffusion. However, if $\mathrm{Pe} \ll 1$—as in many proposed applications for chemistry on the fly [4,5,7]—the microswimmer is essentially static with respect to the transported species, and we do not expect any diffusivity enhancement. In other words, the motility of such swimming catalysts may be irrelevant due to the high diffusion of the reagents of interest [16], a point already well elaborated upon by Purcell and Berg [67–69].

Nevertheless, allowing reasonable values of Pe, we then evaluate the Damköhler Da and Sherwood Sh numbers. $\mathrm{Da} = \kappa l/D$ details the balance between the reaction rate κ and the (diffusive) mass transfer process. Notably, the classical continuum phoretic framework to describe chemical microswimmer motion presumes reaction-rate limited kinetics, i.e., $\mathrm{Da} \to 0$ [33,58,70,71], with finite values of Da leading to decreasing microswimmer speeds [57]—calling into question the goal of overcoming mass-transfer limitations in reactions using microswimmer motility [4,5,7]. Regardless, assuming transport-limited reactions, we examine the Sherwood number for mass transfer to a sphere in Stokes flow, $\mathrm{Sh} = 2 + 0.991\mathrm{Re}^{1/3}\mathrm{Sc}^{1/3}$ [72,73], where $\mathrm{Sc} = \nu/D$ is the Schmidt number (the ratio of momentum to mass diffusivity), the first term is for the asymptotic limit of molecular diffusivity, and $0.991\mathrm{Re}^{1/3}\mathrm{Sc}^{1/3}$ is the advective contribution to mass transport [73]. In creeping flow, we thus expect the enhancement in mass transfer from fluid advection to be small even when $\mathrm{Pe} > 1$ for most physical parameters. In highly viscous reactor settings or when mixing macromolecules with a low diffusivity (or situations combining both features [74]), the microstirrer strategy could be more effective, especially where the microswimmers are large [68,69]. For example, Kim and Breuer [75] demonstrated that *E. coli* could enhance the diffusivity of 77 kDa Dextran (≈10 nm spheres assuming spheres with Stokes-Einstein diffusion) by a factor 4 in a microfluidic chip. Nevertheless, we underline the poor scaling of the Schmidt number with the exponent 1/3, and question whether such modest enhancements in mixing would justify complex reactor designs incorporating motile catalysts.

III. DISCUSSION AND CONCLUSIONS

Basic dimensionless arguments based on convection-reaction-diffusion theory [67–69,76] thus provide some additional insight into the challenges of using autophoretic microswimmers as microstirrers, besides the limitations posed by neglected emergent phenomena such as clustering. Still, it is worth noting that collective behaviors could also enhance fluid intermixing and thereby improve reaction-diffusion limitations [77], while appropriate material selection can modify generated flow fields [78,79] and thereby prevent undesirable aggregation (i.e., for pushers [49,80])—enabling the application of higher microswimmer concentrations. Other promising avenues to increase microswimmer mixing could be achieved via modifying their shape away from classical spheres [81], exploiting bubble generation [82], or multistep procedures making use of different populations of microswimmers [74]. Our results therefore underline the need for a more considered approach to the design and proposed application of synthetic microswimmers to enhance micro- and nanoscale mass transport, and provide evidence that deviations from model (spherical) swimmers may be required for such purposes.

ACKNOWLEDGMENTS

The authors thank M. Popescu and V. Niggel for helpful discussions on theory and experiment, respectively. The authors also thank S. Vasudevan for his assistance with the performed DDM analysis. The authors gratefully acknowledge computing time on the supercomputer JURECA [83] at Forschungszentrum Jülich under the actsys grant.

Author contributions were based on the CRediT (Contributor Roles Taxonomy). Conceptualization: M.R.B., D.A.F., F.P., F.G., G.G., L.I. Funding acquisition: L.I. Investigation and analysis: M.R.B., D.A.F. Methodology: M.R.B., D.A.F., F.P. Supervision: L.I. Visualization and writing: M.R.B., D.A.F., F.P., F.G., G.G., L.I.

[1] S. Ramaswamy, Annu. Rev. Condens. Matter Phys. **1**, 323 (2010).
[2] G. Gompper, R. G. Winkler, T. Speck, A. Solon, C. Nardini, F. Peruani, H. Löwen, R. Golestanian, U. B. Kaupp *et al.*, J. Phys.: Condens. Matter **32**, 193001 (2020).
[3] C. Bechinger, R. Di Leonardo, H. Löwen, C. Reichhardt, G. Volpe, and G. Volpe, Rev. Mod. Phys. **88**, 045006 (2016).
[4] E. Karshalev, B. Esteban-Fernández De Ávila, and J. Wang, J. Am. Chem. Soc. **140**, 3810 (2018).
[5] B. Dai, Y. Zhou, X. Xiao, Y. Chen, J. Guo, C. Gao, Y. Xie, and J. Chen, Adv. Sci. **9**, 2203057 (2022).
[6] L. Wang, A. Kaeppler, D. Fischer, and J. Simmchen, ACS Appl. Mater. Interfaces **11**, 32937 (2019).
[7] M. Wittmann, S. Heckel, F. Wurl, Z. Xiao, T. Gemming, T. Strassner, and J. Simmchen, Chem. Commun. **58**, 4052 (2022).
[8] X. L. Wu and A. Libchaber, Phys. Rev. Lett. **84**, 3017 (2000).
[9] K. C. Leptos, J. S. Guasto, J. P. Gollub, A. I. Pesci, and R. E. Goldstein, Phys. Rev. Lett. **103**, 198103 (2009).
[10] C. Valeriani, M. Li, J. Novosel, J. Arlt, and D. Marenduzzo, Soft Matter **7**, 5228 (2011).
[11] L. G. Wilson, V. A. Martinez, J. Schwarz-Linek, J. Tailleur, G. Bryant, P. N. Pusey, and W. C. K. Poon, Phys. Rev. Lett. **106**, 018101 (2011).
[12] Z. Lin, J.-L. Thiffeault, and S. Childress, J. Fluid Mech. **669**, 167 (2011).
[13] A. Morozov and D. Marenduzzo, Soft Matter **10**, 2748 (2014).
[14] R. Jeanneret, D. O. Pushkin, V. Kantsler, and M. Polin, Nat. Commun. **7**, 12518 (2016).
[15] A. Lagarde, N. Dagès, T. Nemoto, V. Démery, D. Bartolo, and T. Gibaud, Soft Matter **16**, 7503 (2020).
[16] K. Kanazawa, T. G. Sano, A. Cairoli, and A. Baule, Nature (London) **579**, 364 (2020).
[17] J.-L. Thiffeault and S. Childress, Phys. Lett. A **374**, 3487 (2010).
[18] A. S. Mikhailov and R. Kapral, Proc. Natl. Acad. Sci. USA **112**, E3639 (2015).
[19] X. Zhao, K. K. Dey, S. Jeganathan, P. J. Butler, U. M. Córdova-Figueroa, and A. Sen, Nano Lett. **17**, 4807 (2017).
[20] G. Miño, T. E. Mallouk, T. Darnige, M. Hoyos, J. Dauchet, J. Dunstan, R. Soto, Y. Wang, A. Rousselet, and E. Clement, Phys. Rev. Lett. **106**, 048102 (2011).
[21] B. Wang, F. Ji, J. Yu, L. Yang, Q. Wang, and L. Zhang, iScience **19**, 760 (2019).
[22] J. Orozco, B. Jurado-Sánchez, G. Wagner, W. Gao, R. Vazquez-Duhalt, S. Sattayasamitsathit, M. Galarnyk, A. Cortés, D. Saintillan, and J. Wang, Langmuir **30**, 5082 (2014).
[23] M. R. Bailey, F. Grillo, N. D. Spencer, and L. Isa, Adv. Funct. Mater. **32**, 2109175 (2022).
[24] M. R. Bailey, T. A. Gm{ur, F. Grillo, and L. Isa, Chem. Mater. **35**, 3731 (2023).
[25] M. Wittmann, A. Ali, T. Gemming, F. Stavale, and J. Simmchen, J. Phys. Chem. Lett. **12**, 9651 (2021).
[26] J.-L. Thiffeault, Phys. Rev. E **92**, 023023 (2015).
[27] G. L. Miño, J. Dunstan, A. Rousselet, E. Clément, and R. Soto, J. Fluid Mech. **729**, 423 (2013).
[28] A. Jepson, V. A. Martinez, J. Schwarz-Linek, A. Morozov, and W. C. K. Poon, Phys. Rev. E **88**, 041002(R) (2013).
[29] D. O. Pushkin and J. M. Yeomans, Phys. Rev. Lett. **111**, 188101 (2013).
[30] E. W. Burkholder and J. F. Brady, Phys. Rev. E **95**, 052605 (2017).
[31] I. O. Gøtze and G. Gompper, Phys. Rev. E **82**, 041921 (2010).
[32] A. Zöttl and H. Stark, Annu. Rev. Condens. Matter Phys. **14**, 109 (2023).
[33] J. R. Howse, R. A. L. Jones, A. J. Ryan, T. Gough, R. Vafabakhsh, and R. Golestanian, Phys. Rev. Lett. **99**, 048102 (2007).
[34] R. Golestanian, Phys. Rev. Lett. **102**, 188305 (2009).
[35] M. N. Popescu, S. Dietrich, M. Tasinkevych, and J. Ralston, Eur. Phys. J. E **31**, 351 (2010).
[36] K. K. Dey, F. Wong, A. Altemose, and A. Sen, Curr. Opin. Colloid Interface Sci. **21**, 4 (2016).
[37] M. R. Bailey, N. Reichholf, A. Flechsig, F. Grillo, and L. Isa, Part. Part. Syst. Charact. **39**, 2100200 (2022).
[38] See Supplemental Material at http://link.aps.org/supplemental/10.1103/PhysRevE.110.044601 for the experimental and numerical materials and methods, including a detailed description of the hydrodynamic squirmer model used to produce Figs. 3 and 4; definition of microswimmer clusters and the relevant speed distributions; effect of active transport on ensemble tracer dynamics; control experiments performed for tracer displacements; phoretic interactions between Janus pumps and tracers; tracer dynamics in the presence of Janus pumps; nanoparticle tracer dynamics in a Janus microswimmer bath; and videos showing the motion of dilute and dense suspensions of particles and their effect on tracer displacements
[39] M. R. Bailey, F. Grillo, and L. Isa, Soft Matter **18**, 7291 (2022).
[40] M. Bailey, C. M. Barriuso Gutierrez, J. Martin-Roca, V. Niggel, V. Carrasco Fadanelli, I. Buttinoni, I. Pagonabarraga, L. Isa, and C. Valeriani, Nanoscale **16**, 2444 (2024).
[41] I. Theurkauff, C. Cottin-Bizonne, J. Palacci, C. Ybert, and L. Bocquet, Phys. Rev. Lett. **108**, 268303 (2012).
[42] S. Thakur and R. Kapral, Phys. Rev. E **85**, 026121 (2012).
[43] J. Palacci, S. Sacanna, A. P. Steinberg, D. J. Pine, and P. M. Chaikin, Science **339**, 936 (2013).
[44] B. M. Mognetti, A. Šarić, S. Angioletti-Uberti, A. Cacciuto, C. Valeriani, and D. Frenkel, Phys. Rev. Lett. **111**, 245702 (2013).
[45] B. Liebchen, D. Marenduzzo, and M. E. Cates, Phys. Rev. Lett. **118**, 268001 (2017).
[46] F. Ginot, I. Theurkauff, F. Detcheverry, C. Ybert, and C. Cottin-Bizonne, Nat. Commun. **9**, 696 (2018).
[47] X. Chen, X. Dong, A. Be'er, H. L. Swinney, and H. P. Zhang, Phys. Rev. Lett. **108**, 148101 (2012).
[48] X. Chen, X. Yang, M. Yang, and H. P. Zhang, Europhys. Lett. **111**, 54002 (2015).
[49] M. Theers, E. Westphal, K. Qi, R. G. Winkler, and G. Gompper, Soft Matter **14**, 8590 (2018).
[50] F. Mou, L. Kong, C. Chen, Z. Chen, L. Xu, and J. Guan, Nanoscale **8**, 4976 (2016).
[51] L. Baraban, M. Tasinkevych, M. N. Popescu, S. Sanchez, S. Dietrich, and O. G. Schmidt, Soft Matter **8**, 48 (2012).
[52] J. Palacci, S. Sacanna, A. Vatchinsky, P. M. Chaikin, and D. J. Pine, J. Am. Chem. Soc. **135**, 15978 (2013).
[53] F. Mou, J. Zhang, Z. Wu, S. Du, Z. Zhang, L. Xu, and J. Guan, iScience **19**, 415 (2019).
[54] A. J. T. M. Mathijssen, R. Jeanneret, and M. Polin, Phys. Rev. Fluids **3**, 033103 (2018).
[55] M. J. Lighthill, Commun. Pure Appl. Math. **5**, 109 (1952).
[56] J. R. Blake, Math. Proc. Cambridge Philos. Soc. **70**, 303 (1971).

[57] S. Michelin and E. Lauga, J. Fluid Mech. **747**, 572 (2014).
[58] M. N. Popescu, W. E. Uspal, Z. Eskandari, M. Tasinkevych, and S. Dietrich, Eur. Phys. J. E **41**, 145 (2018).
[59] J. Katuri, W. E. Uspal, M. N. Popescu, and S. Sánchez, Sci. Adv. **7**, eabd0719 (2021).
[60] A. I. Campbell, S. J. Ebbens, P. Illien, and R. Golestanian, Nat. Commun. **10**, 3952 (2019).
[61] M. Yang, A. Wysocki, and M. Ripoll, Soft Matter **10**, 6208 (2014).
[62] I. P. Madden, L. Wang, J. Simmchen, and E. Luijten, Small **18**, 2107023 (2022).
[63] P. J. Hoogerbrugge and J. M. Koelman, Europhys. Lett. **19**, 155 (1992).
[64] P. Español and P. Warren, Europhys. Lett. **30**, 191 (1995).
[65] F. Alarcón, C. Valeriani, and I. Pagonabarraga, Soft Matter **13**, 814 (2017).
[66] S. E. Spagnolie and E. Lauga, J. Fluid Mech. **700**, 105 (2012).
[67] E. M. Purcell, Am. J. Phys. **45**, 3 (1977).
[68] H. Berg and E. Purcell, Biophys. J. **20**, 193 (1977).
[69] E. M. Purcell, J. Fluid Mech. **84**, 551 (1978).
[70] P. Kreissl, C. Holm, and J. De Graaf, J. Chem. Phys. **144**, 204902 (2016).
[71] A. Domínguez and M. N. Popescu, Curr. Opin. Colloid Interface Sci. **61**, 101610 (2022).
[72] S. Friedlander, AIChE J. **7**, 347 (1961).
[73] P. M. Armenante and D. J. Kirwan, Chem. Eng. Sci. **44**, 2781 (1989).
[74] N. Ruiz-González, D. Esporrín-Ubieto, A. C. Hortelao, J. C. Fraire, A. C. Bakenecker, M. Guri-Canals, R. Cugat, J. M. Carrillo, M. Garcia-Batlletbó, P. Laiz, T. Patiño, and S. Sánchez, Small **20**, 2309387 (2024).
[75] M. J. Kim and K. S. Breuer, Phys. Fluids **16**, L78 (2004).
[76] T. M. Squires, R. J. Messinger, and S. R. Manalis, Nat. Biotechnol. **26**, 417 (2008).
[77] Q. Wang, F. Ji, S. Wang, and L. Zhang, ChemNanoMat **7**, 600 (2021).
[78] J. Katuri, W. E. Uspal, J. Simmchen, A. Miguel-López, and S. Sánchez, Sci. Adv. **4**, eaao1755 (2018).
[79] P. Sharan, Z. Xiao, V. Mancuso, W. E. Uspal, and J. Simmchen, ACS Nano **16**, 4599 (2022).
[80] K. Qi, E. Westphal, G. Gompper, and R. G. Winkler, Commun. Phys. **5**, 49 (2022).
[81] K. Xiong, J. Lin, Q. Chen, T. Gao, L. Xu, and J. Guan, Matter **6**, 907 (2023).
[82] R. Mundaca-Uribe, M. Holay, A. Abbas, N. Askarinam, J. S. Sage-Sepulveda, L. Kubiatowicz, R. H. Fang, L. Zhang, and J. Wang, ACS Nano **17**, 9272 (2023).
[83] P. Thørnig, J. Large-Scale Res. Facil. **7**, A182 (2021).